

Lanthanide–organic framework based on a 4,4-(9,9-dimethyl-9H-fluorene-2,7-diyl) dibenzoic acid: Synthesis, structure and fluorescent sensing for a variety of cations and anions simultaneously

Bing Li, Jun Zhou, Fengying Bai*, Yongheng Xing**

College of Chemistry and Chemical Engineering, Liaoning Normal University, Huanghe Road 850#, Dalian, 116029, PR China

ARTICLE INFO

Keywords:

Lanthanide organic frameworks
4,4-(9,9-dimethyl-9H-fluorene-2,7-diyl)
dibenzoic acid (H₂DLDA)
Crystal structure
Fluorescence sensing
Mechanism

ABSTRACT

Based on the structural diversity and the superior luminescence properties of 4,4-(9,9-dimethyl-9H-fluorene-2,7-diyl) dibenzoic acid (H₂DLDA), a series of new lanthanide coordination compounds [Ln(DLDA)(DMF)(H₂O)(COO)]_n (Sm (1), Eu (2), Ce (3), Nd (4), Gd (5)) were successfully prepared by the reaction of H₂DLDA, which is a new type ligand synthesized by structural modification of fluorene, with rare earth metal ion. They were characterized by elemental analysis, IR, TG, PXRD, UV–vis, etc. Analysis results show that the coordination compounds are isomorphous. In particular, the structure of the coordination compound **1** was determined by single crystal X-ray diffraction. The structure analysis shows that compound **1** is a novel 3D supramolecular network structure, and the central metal adopts the eight-coordination mode to form a double-cap triangular prism spatial configuration. It is worth mentioning that the excellent heat-resisting ability of the framework, which is stable until heated to nearly 400 °C. Meanwhile, the fluorescence sensing test showed that as synthesized compound **2** was a new type of fluorescent probe with high efficiency, high selectivity and has the ability to simultaneously detect a variety of cations and anions (Fe³⁺, Al³⁺, Cr³⁺, C₂O₄²⁻, Cr₂O₇²⁻, MnO₄⁻, PO₄³⁻). Moreover, it owns higher K_{sv} value (1.77 × 10⁴ M⁻¹, 1.44 × 10⁴ M⁻¹, 3.621 × 10⁴ M⁻¹, 2.07 × 10³ M⁻¹, 5.65 × 10³ M⁻¹, 3.18 × 10³ M⁻¹, 1.82 × 10³ M⁻¹, respectively) and a lower detection limit (1.93 μM, 2.38 μM, 0.945 μM, 16.5 μM, 6.06 μM, 10.8 μM, 18.8 μM, respectively). This results in compound **2** being superior to other probes reported previously, and the mechanism of fluorescence quenching was explained to some extent. In addition, during the fluorescence titration experiment, we found an interesting luminescence change of compound **2**. Most notably, it emitted white light in DMA solvent under the irradiation of handheld ultraviolet lamp (wavelength: 365 nm) while the solid sample emitted yellow light at the same conditions.

1. Introduction

Coordination compounds (CPs) are a new type of inorganic-organic hybrid materials with one-dimensional, two-dimensional or three-dimensional structures [1–3], which take metal ions or metal clusters as nodes, organic ligands as link units [4–8], and is constructed by means of self-assembly through covalent bond or non-covalent bond connections [9,10]. In recent years, due to the advantages of adjustable structure and size, excellent thermal and chemical stability [11–15], CPs have attracted great attention in the fields of gas storage, catalysis, optics, electricity, magnetism and biomedicine [16–21]. Compared with transition metals, lanthanide metal coordination compounds (CPs) have become research hot spot for many researchers due to their narrow emission bands, large stock shift, high color purity, and long

luminescence lifetime in the field of fluorescence sensing [22–24]. In addition, compared to other traditional detection methods such as ICP-MS, FAAS and spectrophotometric detection [25–28], Ln-CPs is recognized and widely used as a fluorescent probe because of its ease of operation, high selectivity, sensitivity and cyclic stability [29–32].

Fluorene and its derivatives have been widely concerned [32,33] owing to their structurally easy transformation by introducing different functional groups together with excellent electrical, optical properties, thermal stability and chemical stability [34–37], and make them widely used in light-emitting materials, laser device, catalytic materials, magnetic materials, photovoltaic cells, light-emitting diodes (leds), biological sensor devices, biological medicine and adsorption, etc. [38–41]. The luminescent properties of fluorene derivatives are closely related to their molecular structures and electronic properties [42,43].

* Corresponding author. Tel.: +86 0411 82156987.

** Corresponding author.

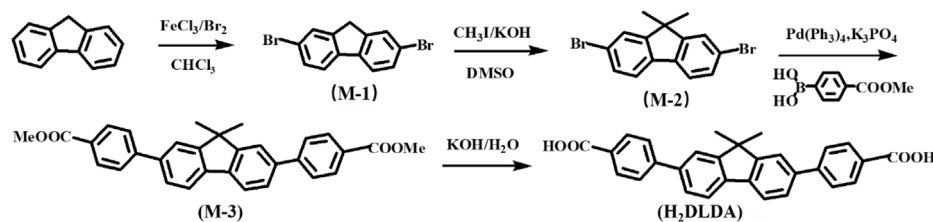
E-mail addresses: baifengying2003@163.com (F. Bai), xingyongheng2000@163.com (Y. Xing).

<https://doi.org/10.1016/j.dyepig.2019.107862>

Received 29 June 2019; Received in revised form 31 August 2019; Accepted 4 September 2019

Available online 05 September 2019

0143-7208/ © 2019 Elsevier Ltd. All rights reserved.



Scheme 1. Synthetic route of H_2DLDA : 2,7-dibromofluorene (M-1); 9, 9-dimethyl-2,7-dibromofluorene (M-2); 9,9-dimethyl-2,7-bis(4-methoxycarbonylphenyl) fluorene(M-3); 4, 4'-(9,9-dimethyl-9H-fluorene-2, 7-diyl) dibenzoic acid (H_2DLDA).

Therefore, new luminescent derivatives of fluorene are designed and synthesized by various new strategies to change the molecular structures of fluorene or change the electron cloud density of its plane [44,45]. For example, Prof. Zhou X. research group reported two coordination polymers (Mg-DLDA and Zn-DLDA) synthesized from 4,4'-(9,9-dimethyl-9H-fluorene-2,7-diyl) dibenzoic acid (H_2DLDA) with Mg (II) or Zn (II) salts. Both the polymers exhibit strong ligand-centered blue emission and the second-order nonlinear optical effects [46]. Inspired by this work, we also designed a series of new Ln-CPs by rare earth metals combined with 4,4'-(9,9-dimethyl-9H-fluorene-2,7-diyl) dibenzoic acid, which is a new fluorene derivatives introducing two methyl groups at position of 9 and phenyl carboxyl group at positions of 2 and 7 of fluorene. By introducing polyaromatic ring and electron donor group into fluorene structure, conjugate structure is increased and planar rigidity is improved, so as to increase the density of electron cloud of the whole molecule skeleton and make it easier for electrons to be excited and fluorescence to be generated.

With the increasing of human production activities, more and more pollutants such as metal ions (Fe^{3+} , Al^{3+} , Cr^{3+} , Cu^{2+} , Pb^{2+} and Hg^{2+} , etc.) [47–50], anions ($Cr_2O_7^{2-}$, MnO_4^- , $C_2O_4^{2-}$, PO_4^{3-} , SO_4^{2-} and NO_3^- , etc.) [51–53] and toxic molecules (such as some small molecule nitro compounds) are released into the soil, the water without restraint, which not only greatly damaged the ecological environment, but also posed a great threat to the living environment of animals and plants [54–57]. How to detect these pollutants efficiently, quickly and simply at the same time has become an urgent problem to be solved in today's society. As is known to all, CPs can exhibit a wide range of luminescent behaviors originating from the multifaceted nature of their structure, that make CPs materials ideal for sensing applications [58]. However, the vast majority of Ln-CPs that have been reported focus on detecting a specific single substance, and few reports can detect multiple substances or substances under different systems simultaneously [59–61]. But most contaminated ions often do not exist alone, causing the limitations of this detection probe application. So, exploiting Ln-CPs for the detection of mixture ions still remains a great challenge. Therefore, how to design and synthesize a multi-functional probe material that can detect multiple substances at the same time has become an urgent need at present. In this context, we successfully synthesized a series of new Ln-fluorene framework CPs by the reaction of lanthanide metal ions (Sm (1), Eu (2), Ce (3), Nd (4), Gd (5)) and organic ligand 4,4'-(9,9-dimethyl-9H-fluorene-2,7-diyl) dibenzoic acid. In particular, Eu-phenyl carboxyl fluorene framework CP (2) has been proved by fluorescence detection test to be able to exhibits multi-responsive behavior towards Fe^{3+} , Al^{3+} , Cr^{3+} and $C_2O_4^{2-}$, $Cr_2O_7^{2-}$, MnO_4^- , PO_4^{3-} in the solution with a rapid response, extremely high quenching efficiency and stability. As far as we know, the Ksv and detection limit of Eu-DLDA are better than that reported previously Ln-CPs, so it can be a promising fluorescent probe [62–65].

2. Experimental section

2.1. Materials and methods

All the chemicals purchased were of reagent grade or better and

were used without further purification. Ligand H_2DLDA was successfully synthesized with reference to relevant literature. IR spectra were performed using a Bruker AXS TENSOR-27 FT-IR spectrometer with pressed KBr pellets in the range of $400\text{--}4000\text{ cm}^{-1}$. The elemental analyses of C, H, and N were carried out with a PerkinElmer 240C automatic analyzer. Thermogravimetric analyses (TG) were performed under the condition of N_2 atmosphere at a heating rate of $10\text{ }^\circ\text{C min}^{-1}$ using a PerkinElmer Diamond TG/DTA. The photoluminescent spectra of the coordination polymers were measured on a HORIBA Fluoromax-4-TCSPC spectrofluorometer equipped with Spectra LED Pulsed LED sources at room temperature (200–1000 nm) with 3.2-inch Integrating Sphere that can be installed in seconds replacing standard cuvette holder. UV–vis spectra were recorded with JASCO V-570 spectrophotometer with Integrating Sphere ($\Phi = 60\text{ mm}$) that can be installed in standard cuvette holder (200–2500 nm, in the form of solid sample) and Lambda 35 UV–vis Spectrometer (200–800 nm). PXRD patterns were obtained with a Bruker Advance-D8 equipped with Cu-K α radiation, in the range of $5^\circ < 2\theta < 60^\circ$, with a step size of 0.02° (2θ) and a count time of 2 s per step.

2.2. Preparation

2.2.1. Preparation of the H_2DLDA

Ligand (H_2DLDA) was synthesized on the basis of the method in related literatures [66,67], see the supplementary materials for specific synthesis methods (Section 1). The synthetic route is as follows Scheme 1.

2.2.2. The characterization data of H_2DLDA and intermediates [67]

2,7-dibromofluorene (M-1), white needle crystal, mass 15.55 g, yield 80%, m.p./ $^\circ\text{C}$: 164–165. IR data (KBr, ν/cm^{-1}): 3054 (=CH-stretching); 2922, 2855 (C–H stretching); 1599, 1573, 1451 (ph skeleton vibration); 1396 (C–H bending). $^1\text{H NMR}$: δH (CDCl_3 , 500 MHz, δ/ppm): 7.61 (2H, s, Ar), 7.53 (2H, d, $J = 8.1\text{ Hz}$, Ar), 7.46 (2H, dd, $J_1 = 8.1\text{ Hz}$, $J_2 = 1.5\text{ Hz}$, Ar), 3.79 (2H, s, CH_2). $^{13}\text{C NMR}$ (CDCl_3 , 300 MHz, δ/ppm): 144.8, 139.7, 130.1, 128.3, 121.2, 120.9, 36.5. Elemental analyses: Found: C, 48.03; H, 2.45%; molecular formula $\text{C}_{13}\text{H}_8\text{Br}_2$ requires C, 48.18; H, 2.47%.

9, 9-dimethyl-2,7-dibromofluorene (M-2), yellow acicular crystals, mass: 11.40 g, yield 81%, m.p./ $^\circ\text{C}$: 179–180. IR data (KBr, ν/cm^{-1}): 3027 (=CH-stretching); 2965, 2922, 2865 (C–H stretching); 1596, 1575, 1448 (ph skeleton vibration); 1398 (C–H bending). $^1\text{H NMR}$: δH (CDCl_3 , 500 MHz, δ/ppm): 7.53–7.51 (4H, m, Ar), 7.44 (2H, dd, $J_1 = 8.1\text{ Hz}$, $J_2 = 1.2\text{ Hz}$, Ar), 1.45 (6H, s, 2 CH_3). $^{13}\text{C NMR}$ (CDCl_3 , 300 MHz, δ/ppm): 155.2, 137.2, 130.3, 126.2, 121.5, 121.4, 47.3, 26.8. Elemental analyses: Found: C, 51.16, H, 3.39%; molecular formula $\text{C}_{15}\text{H}_{12}\text{Br}_2$ requires C, 51.17; H, 3.41%.

9,9-dimethyl-2,7-bis(4-methoxycarbonylphenyl) fluorene (M-3), white powdery solid, mass: 3.72 g, yield: 50%, m.p./ $^\circ\text{C}$: > 200. IR data (KBr, ν/cm^{-1}): 3069 (=CH-stretching); 2954, 2924, 2853 (C–H stretching); 1724 (C=O stretching); 1610, 1438 (ph skeleton vibration); 1398 (C–H bending); 1286 (C–O–C asymmetric stretching).

$^1\text{H NMR}$: δH (CDCl_3 , 500 MHz, δ/ppm): 8.14 (4H, d, $J = 8.0\text{ Hz}$, Ar), 7.84 (2H, d, $J = 7.8\text{ Hz}$, Ar), 7.75 (4H, d, $J = 8.0\text{ Hz}$, Ar), 7.70 (2H, d,

$J = 1.0$ Hz, Ar), 7.64 (2H, dd, $J_1 = 7.8$ Hz, $J_2 = 1.0$ Hz, Ar), 3.99 (6H, s, 2 OCH₃), 1.54 (6H, s, 2 CH₃).

¹³C NMR (DMSO-*d*₆, 125 MHz, δ /ppm): 166.27, 155.99, 142.14, 138.52, 137.51, 131.20, 130.27, 129.23, 127.04, 121.60, 120.60, 52.45, 47.32, 27.04. Elemental analyses: Found: C, 80.52; H, 5.64%; molecular formula C₃₁H₂₆O₄ requires C, 80.50; H, 5.67%.

4, 4-(9,9-dimethyl-9H-fluorene-2, 7-diyl) dibenzoic acid (H₂DLDA), white powdery solid, mass: 1.125 g, yield: 90%, m.p./°C: > 200. IR data (KBr, ν /cm⁻¹): 3413 (O–H stretching); 3057 (=CH– stretching); 2956, 2926, 2855 (C–H stretching); 1683 (C=O stretching); 1594, 1504, 1447 (ph skeleton vibration); 1386 (C–H bending); 1285 (C–O stretching). ¹H NMR (DMSO-*d*₆, 500 MHz, δ /ppm): 12.91 (2H, s, 2 COOH), 8.05 (4H, d, $J = 8.1$ Hz, Ar), 8.00–7.98 (4H, m, Ar), 7.91 (4H, d, $J = 8.1$ Hz, Ar), 7.76 (2H, d, $J = 7.9$ Hz, Ar), 1.58 (6H, s, 2 CH₃). ¹³C NMR (DMSO-*d*₆, 125 MHz, δ /ppm): 167.12, 154.72, 144.52, 138.38, 138.15, 129.89, 129.41, 126.83, 126.20, 121.45, 120.98, 46.87, 26.70. Elemental analyses: Found: C, 80.15; H, 5.07%; molecular formula C₂₉H₂₂O₄ requires C, 80.17; H, 5.10%.

2.2.3. Preparation of the compounds

0.0222 g of Sm(NO₃)₃·6H₂O (0.05 mmol) and 0.0221 g of H₂DLDA (0.05 mmol) were dissolved in a mixture solution containing 5 mL of DMF, 2 mL of EtOH and 1 mL of H₂O, then, dilute nitric acid was used to adjust the pH of the solution to 6–7. After stirring at room temperature for 2 h, the mixture solution was put into Teflon-lined stainless steel autoclave and heated at 120 °C for 4 days, finally, cooled to room temperature, light yellow transparent crystals were obtained by washing with ethanol. The synthesis procedures of the compounds 2–5 are similar to that of compound 1, except that the rare earth nitrates used are different. Detailed elemental analysis and infrared data are as follows:

[Sm(DLDA)(DMF)(H₂O)(COO)]_n (1) Mass obtained: 20.10 mg. Yield: 56% (based on Sm³⁺). IR data (KBr, cm⁻¹): 3447, 3124, 2959, 2861, 1673, 1590, 1409, 1282, 823, 765. Elemental Analyses: Found: C, 55.08; H, 4.14; N, 1.92%; molecular formula C₃₃H₃₀NO₈Sm requires C, 55.12; H, 4.18; N, 1.95%.

[Eu(DLDA)(DMF)(H₂O)(COO)]_n (2) Mass obtained: 16.92 mg. Yield: 47% (based on Eu³⁺). IR data (KBr, cm⁻¹): 3447, 3074, 2959, 2863, 1681, 1599, 1409, 1285, 853, 778. Elemental Analyses: Found: C, 54.98; H, 4.15; N, 1.91%; molecular formula C₃₃H₃₀NO₈Eu requires C, 55.01; H, 4.17; N, 1.94%.

[Ce(DLDA)(DMF)(H₂O)(COO)]_n (3) Mass obtained: 15.22 mg. Yield: 43% (based on Ce³⁺). IR data (KBr, cm⁻¹): 3455, 3127, 2963, 2859, 1680, 1599, 1408, 1286, 817, 765. Elemental Analyses: Found: C, 55.88; H, 4.19; N, 1.95%; molecular formula C₃₃H₃₀NO₈Ce requires C, 55.92; H, 4.24; N, 1.98%.

[Nd(DLDA)(DMF)(H₂O)(COO)]_n (4) Mass obtained: 13.88 mg. Yield: 39% (based on Nd³⁺). IR data (KBr, cm⁻¹): 3448, 3155, 2914, 2841, 1650, 1570, 1401, 1248, 834, 780. Elemental Analyses: Found: C, 55.58; H, 4.19; N, 1.94%; molecular formula C₃₃H₃₀NO₈Nd requires C, 55.60; H, 4.21; N, 1.97%.

[Gd(DLDA)(DMF)(H₂O)(COO)]_n (5) Mass obtained: 14.14 mg. Yield: 39% (based on Gd³⁺). IR data (KBr, cm⁻¹): 3455, 3132, 2958, 2863, 1672, 1599, 1404, 1286, 817, 765. Elemental Analyses: Found: C, 54.58; H, 4.11; N, 1.90%; molecular formula C₃₃H₃₀NO₈Gd requires C, 54.60; H, 4.14; N, 1.93%.

2.3. X-ray crystal structure determination

Suitable single crystal of the compound 1 was mounted on glass fibers for X-ray measurement. Reflection data were collected at room temperature on a Bruker AXS SMART APEX II CCD diffractometer with graphite monochromatized Mo-K α radiation ($\lambda = 0.71073$ Å). A semi-empirical absorption correction was applied by the program SADABS [68]. The program suite SHELXTL-97 was used for space-group determination (XPREP), direct method structure solution (XS), and least-

squares refinement (XL) [69,70]. All non-hydrogen atoms were refined with anisotropic displacement parameters. The positions of the hydrogen atoms around the carbon atoms were included using a riding model. Hydrogen atoms of coordination water molecules and lattice water molecules were found in the difference Fourier map. Crystal data and structural refinement parameters are given in Table S1 and selected bond lengths and angles of the compound 1 are listed in Table S2. Since the single crystal quality of the compounds 2, 3, 4 and 5 is poor and is not suitable the requirements of X-ray single crystal diffraction test, unfortunately, we have not obtained their precise single crystal structure as desired, however, by microanalysis (elemental analysis, IR, PXRD) and research experience, it could still prove that they are isomorphous.

3. Results and discussion

3.1. Synthesis

Compound 1–5 are obtained under hydrothermal conditions by heating mixture solution contained rare earth nitrate salt and H₂DLDA for 4 days. Furthermore, attempts to vary other synthetic parameters such as pH value, molar ratio of the reactants and the identity of the base are also unsuccessful, only producing some precipitates or microcrystalline products (2–5) that are unsuitable for single crystal X-ray diffraction analysis owing to making rapid aggregates except for 1. In order to obtain the expected the better crystalline conditions of the compounds, we mainly regulate from several aspects that affect the reaction. The first is the environment of the reaction. The experiments prove that hydrothermal synthesis is the optimum reaction conditions. Secondly, we separately compare the molar ratio of the reactants, the solvent selection and the dosage, the pH value of the system, the reaction temperature and the reaction time. During a mass of the experiments, we found that the selected solvent and the reaction temperature play vital roles in the reaction process, so we tried different reagents as solvents, and finally came to the conclusion that the mixed solvents composed of DMF, EtOH and H₂O were the best reaction system, and their volume ratios are also regulated. Besides, through different temperature attempts, such as 80, 100, 120, 140, 160 °C and it was found finally at 120 °C to obtain the crystalline of the target compounds.

3.2. IR spectra

By infrared spectroscopy analysis, the broader absorption band at 3447 cm⁻¹ of compound 1 shown the presence of water molecules. The peak position at 1673 cm⁻¹ and 1409 cm⁻¹ can be attributed to the asymmetric stretching vibration of the C=O bond (ν_{asCOO^-}) and the C=O symmetric stretching vibration (ν_{sCOO^-}), and compared to main position of the carboxyl peak at 1684 cm⁻¹ of the ligand H₂DLDA, a red shift occurred, indicating that the metal atom coordinated with the ligand. Detailed infrared spectral data of compounds 1–5 are shown in Table S4. The infrared spectra of all compounds are shown in Fig. S1.

3.3. PXRD analyses

The PXRD spectra of compounds 1–5 were obtained and compared with that of the corresponding simulated from single crystal data. As shown in Fig. S2. The measured peaks of compounds 1–5 are very consistent with the simulated values, and there were no other peaks, indicating compounds 1–5 are pure phase. In addition, the peak positions of compounds 1–5 are identical, indicating that they are isomorphous compounds. The different intensity may be due to the preferred orientation of the powder samples.

3.4. Thermal properties

In order to confirm the thermal stability of the compounds, thermogravimetric analysis was carried out under a N_2 atmosphere at a temperature increase rate of $10\text{ }^\circ\text{C min}^{-1}$, and the temperature range was $30\text{--}1000\text{ }^\circ\text{C}$. It can be seen from the PXRD spectrum that the five compounds are isomorphous compounds with only different metals, so we selected the compound **1** as a representative for thermogravimetric data analysis. TG curve of compound **1** can be divided into three stages of weight loss. The weight loss of the first stage occurs in the temperature rising process from room temperature to $370\text{ }^\circ\text{C}$, the weight loss is about 4.20%, which should be the loss of the coordination water and the partially coordinated DMF molecules. The weight loss in the second stage occurs at $370\text{--}480\text{ }^\circ\text{C}$, the weight loss is about 59.75%, it could be attributed to the loss of residual DMF and partial H_2DLDA ligand; the third stage the weight loss occurs during the temperature rise of $480\text{--}1000\text{ }^\circ\text{C}$, and the weight loss is about 11.80%, the weight loss at this stage may be due to the loss of the remaining ligands. At this point, the framework of the compound collapses, eventually remaining the metal oxide. The compound began to lose weight in the first stage when the temperature was nearly $400\text{ }^\circ\text{C}$, which indicated that the thermal stability of the compound is stable and has good application value, which provided theoretical support for the following related research work. Thermogravimetric diagrams of the five compounds are shown in Fig. S3, comparison of TG curves shows that their composition is similar.

3.5. Structure descriptions

$[Sm(DLDA)(DMF)(H_2O)(COO)]_n$ (**1**) Compound **1** is an orthorhombic system, $Pna2_1$ space group, and composed of one Sm atom, one coordinated H_2DLDA ligand and one DMF molecule, and one water molecule and two coordinated carboxyl group from formic acid, which maybe come from decomposing of the DMF solvent [71]. Fig. 1a shows the coordination environment of the center metal Sm. In each structural unit, there are eight coordinating sites around the center metal Sm, coordinated atoms derived from carboxyl oxygen (O8) in the coordinated DMF molecules, four oxygen atoms in two para-carboxyl groups of the deprotonated ligand DLDA (O1, O2, O3, O4), two molecules of deprotonated carboxyl oxygen atoms (O5^{#1}, O6; #1: $x, y, z-1$), and remaining one site is occupied by oxygen atom of water (O7), respectively, forming a double-capped triangular prism spatial configuration. In the structure of compound **1**, there are three different types of Sm–O bonds, the details are as follows: (i) Sm–O bond formed by the

carboxyl oxygen atom from the ligand DLDA (O1, O2, O3 and O4) and Sm, the bond lengths are 2.522(5) Å, 2.430(6) Å, 2.554(11) Å, 2.444(10) Å, respectively. (ii) Sm–O bond formed between carboxyl oxygen atoms in formic acid generated by solvent decomposition (O5^{#1}, O6; #1: $x, y, z-1$) and Sm, and the bond lengths between them are 2.312(10) Å, 2.391(11) Å, respectively. (iii) Sm–O bond composed of oxygen atoms in coordination molecules DMF (O8), H_2O (O7) and Sm. The bond lengths are 2.407(6) Å, 2.425(6) Å. Compared to the Sm–O bond length ranges from 2.337(5) Å to 2.958(5) Å of the reported compound $[Sm_2(HPI_2C)_3(DMF)_2(H_2O)_2]\cdot 2DMF(H_3PI_2C = (5-(2-(2-hydroxyphenyl)-4,5-diphenyl-1H-imidazol-1-yl)isophthalic\ acid))$ [72], the Sm–O bond length range of the compound **1** is 2.312(10) Å to 2.554(11) Å, which is slightly shorter. In order to better understand the structure of the compound, the twist angle of adjacent benzene rings in the compound was calculated by program of SHELXTL-97. The twist angle between the benzene ring I (C2–C7) and the benzene ring II (C8–C13) is 37.8 (8) degrees, and the twist angle between the benzene ring III (C17–C22) and the benzene ring IV (C23–C28) is 30.9 (7) degrees. In addition, the dihedral angle $\angle\alpha$ (composed of C6 C5 C8 C13) is 42 (2) degrees, and the dihedral angle $\angle\beta$ (composed of C22 C21 C23 C28) is 31 (2) degrees.

The deprotonated ligand DLDA is connected in the manner of $\mu_2\text{-}\eta^2\eta^2$, in which two oxygen atoms on each carboxyl group are coordinated to the metal atom in a bidentate chelation mode. In the packing structure, a repeating structural unit can be described as $[Sm(\mu\text{-COO})_2O_3DMF]$, and it is found that along the a -axis direction, the adjacent unit are connected to each other through carbon atom in the DLDA molecule to form a one-dimensional chain, and then a two-dimensional network on the ac plane is formed by longitudinal linking the chain via the metal-coordinated deprotonated carboxyl group along the c axis (Fig. 1b). In addition, the one-dimensional chain extends in the direction of b axis through the connection of hydrogen bond O7–H1A...O4, forming a 2D network on the ab plane, then, through the linking of hydrogen bond O7–H1B...O3, the 2D network on plane ab packing along the direction of c axis furthermore extend and eventually form a 3D supramolecular network structure. As shown in Fig. 1c. In the packing structure, the maximum contact of Sm...Sm is 24.0587 Å; the minimum contact is 6.7881 Å. Detailed hydrogen bond data are list in Table S3.

3.6. Solid UV–vis absorption spectra

The UV–vis absorption spectra of the compound **2** and the ligand H_2DLDA were recorded (See Fig. 2). There are two strong absorption

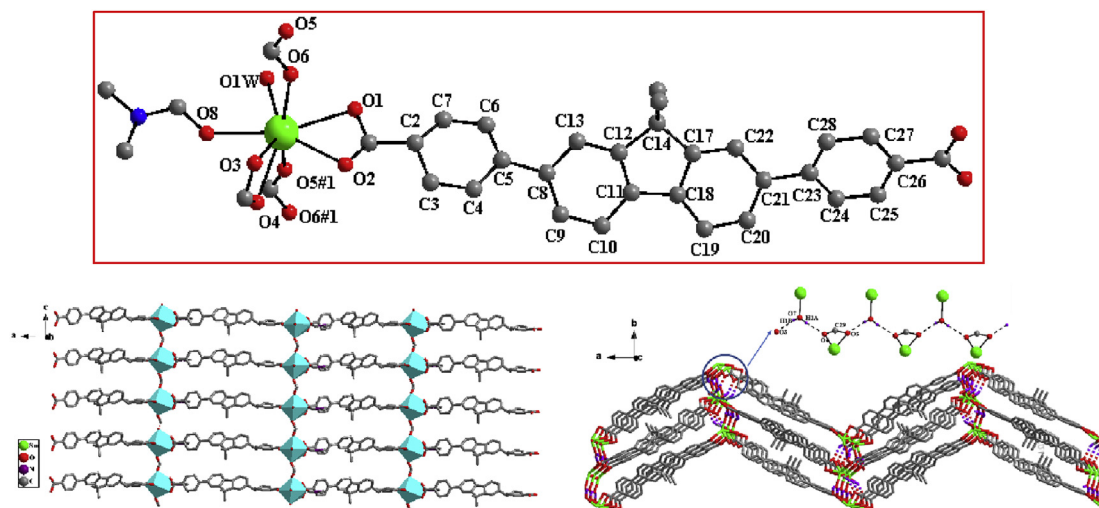


Fig. 1. (a) Coordination environment of the central metal; (b) 2D network structure; (c) 3D supramolecular network structure (note: the illustration is an enlarged view of the hydrogen bonding method).

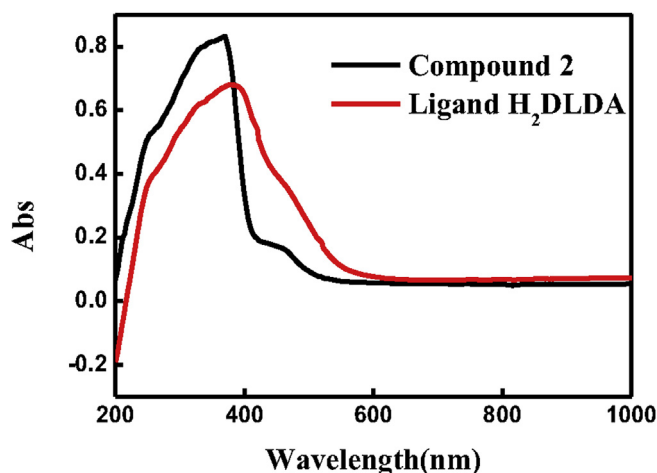


Fig. 2. Solid UV-vis absorption spectra of compound 2 and Ligand H₂DLDA.

bands at 269 nm and 384 nm correspond to the $\pi\text{-}\pi^*$ transition and $n\text{-}\pi^*$ transition of the ligand H₂DLDA. Compound 2 also exhibits two peaks at 251 nm and 367 nm, which are similar to the peaks of the ligand. Since the f-f transition of Eu³⁺ is a spin-forbidden transition, the UV absorption is extremely weak, so in the compound 2, the UV absorption of Eu³⁺ is not observed, therefore, the absorption bands of the compound are predominantly contributed by the ligand H₂DLDA, the UV absorption of compound 2 originated from ligand-to-ligand transition (LLCT), which leads to the UV absorption peak shape and position of the compound and the ligand are similar. Furthermore, the absorption peak of the compound is blue-shifted compared to the ligand, indicating that a coordination reaction occurs between the ligand and Eu³⁺, forming a stable compound. After the compound is formed, the electron cloud on the benzene ring moves toward Eu³⁺, resulting in a decrease in the conjugation and a reduction in rigidity of the benzene ring, so the wavelength shifted blue. The broad peak of the compound near 450 nm should be attributed to the LMCT transition.

3.7. Solid-state photoluminescent spectra

The solid-state fluorescence characterization of the compound 2 and the ligand H₂DLDA was recorded at room temperature (See Fig. 3). Under the monitoring of 614 nm, the excitation spectra of the compound 2 include a wide band at 325–375 nm attributed to $\pi\text{-}\pi^*$ electron transition of organic ligand. At the same time, the narrow peaks at 393 nm, 463 nm, 534 nm, are belong to the energy level transition of

Eu³⁺ ion and the interaction with ligand, because the H₂DLDA exhibits wide absorption in the range of 300–500 nm. These results suggest that the excitation spectra of the compound 2 contain not only the organic ligands $\pi\text{-}\pi^*$ transitions, but also the strong energy level transitions of Eu³⁺ ion. Comprehensive analysis of above information, we know that the contribution to the excitation spectra is not only derived from the electron transition of Eu³⁺ itself, but also partly from the energy transmitted by the antenna effect of the ligand. In the emission spectrum of compound 2 ($\lambda_{\text{ex}} = 358$ nm), several ${}^5\text{D}_0 \rightarrow {}^7\text{F}_J$ ($J = 1\text{--}4$) emission peaks typical of Eu³⁺ ion are observed, and the peak positions of typical emission peaks are 590, 614, 652 and 699 nm, respectively. At 578 nm, the particularly weak emission peak is attributed to ${}^5\text{D}_0 \rightarrow {}^7\text{F}_0$, which is caused by the symmetry-forbidden transition of europium ion. The extremely strong peak at 614 nm belongs to the ${}^5\text{D}_0 \rightarrow {}^7\text{F}_2$ transition, which is an electric dipole transition. Its emission intensity changes significantly with the Eu³⁺ coordination environment, while the ${}^5\text{D}_0 \rightarrow {}^7\text{F}_1$ transition at 590 nm is a magnetic dipole transition. Without any symmetry limitation, its emission intensity is hardly affected by the Eu³⁺ coordination environment, and the ratio of the relative intensity of the ${}^5\text{D}_0 \rightarrow {}^7\text{F}_2$ transition to the ${}^5\text{D}_0 \rightarrow {}^7\text{F}_1$ transition can indicate the symmetry of the central ion lattice. From the emission spectrum of the compound, it can be seen that the ${}^5\text{D}_0 \rightarrow {}^7\text{F}_2$ transition intensity is much stronger than the ${}^5\text{D}_0 \rightarrow {}^7\text{F}_1$ transition intensity, indicating that the central ion Eu³⁺ is in a lower symmetrical environment, which is consistent with the crystal structure of the compound. Meanwhile, the ligand emission spectrum showed wide absorption in the range of 450–550 nm, while the absorption peak appeared in the same position of compound 2, which further indicates that the ligand contributes a certain degree to the luminescence of the compound. Then, the solid compound 2 and the ligand H₂DLDA were respectively irradiated with a handheld ultraviolet lamp, which respectively emit yellow light and yellow green light, and the CIE diagrams are as shown in Fig. S4.

3.8. Fluorescence sensing properties of compound 2

3.8.1. Solvent selection

Our group has been engaged in the functional properties research of fluorene and its derivatives as well as the coordination compounds. Some works about fluorescence sensing properties of ligand H₂DLDA have been reported by us [73]. In order to further investigate the fluorescence properties of the compounds constructed by H₂DLDA, we synthesized above a series of Ln-CPs, among them based on the fluorescence characteristics of Eu³⁺, Eu-DLDA (compound 2) is selected for fluorescence sensing. Therefore, it is first necessary to explore an

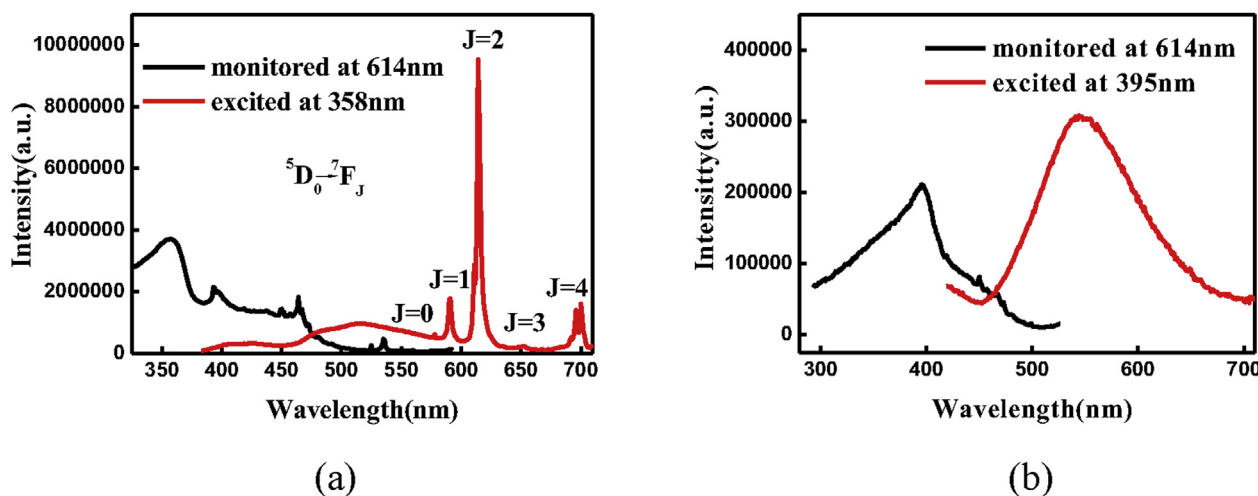


Fig. 3. Solid state fluorescence excitation and emission spectra at room temperature: (a) compound 2; (b) H₂DLDA.

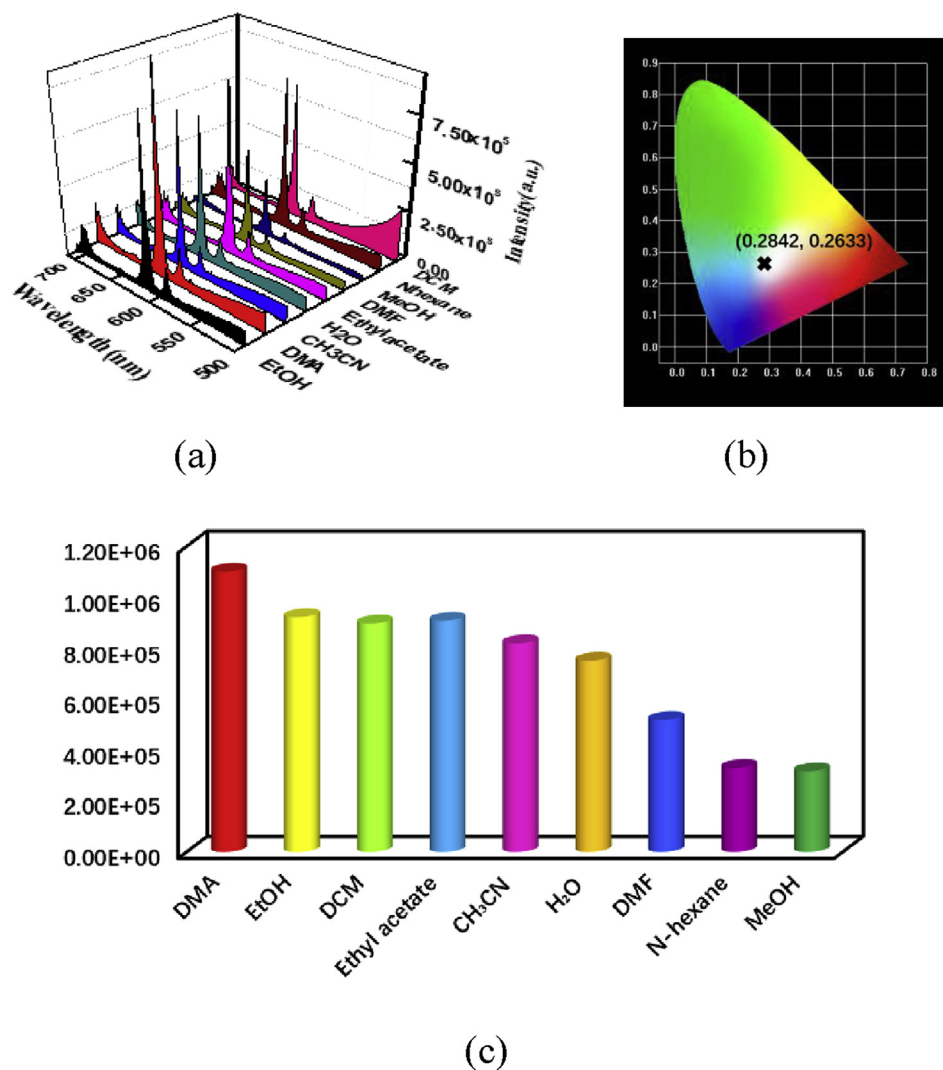


Fig. 4. (a) Fluorescence intensity of compound 2 was compared in different solvent systems; (b) CIE chromaticity diagram of compound 2 in DMA; (c) Fluorescence intensity at 614 nm.

optimal luminescence response of compound 2 in different solvent systems, so compound 2 was dispersed into following nine different solvents (ethanol (EtOH), N,N-Dimethylacetamide (DMA), acetonitrile (CH₃CN), water (H₂O), ethyl acetate, N,N-dimethylformamide (DMF), methanol (MeOH), N-hexane, dichloromethane (DCM)), respectively, ultrasound treatment was performed for 30 min before fluorescence test to ensure the uniform distribution suspension system (the suspension concentration is 1 mg/1 mL). It can be distinctly seen from Fig. 4a that the fluorescence intensity of the compound changes with the solvent difference in the system, but the positions of the maximum emission (614 nm) does not change, showing that different solvent molecules do not affect the excited state energy level of the compound. At the same time, the emission peak intensity at 400–450 nm varies with the solvents, indicating that the solvent has a certain influence on the energy transfer of the ligand, further indicating that this part of the energy in the suspension is not completely transferred to Eu³⁺. In addition, the emission peak intensity of compound 2 at 614 nm was the strongest in DMA, and it also showed strong absorption in the range of 400–450 nm, which is within the wavelength range of blue light. Based on the above considerations DMA is chosen as the most optimized solvent for the following all fluorescence titration experiments. Simultaneously, we also found an interesting luminescence change by using handheld ultraviolet lamp to illuminate the compound 2 dispersed in the DMA, emitting a white light. CIE diagram as shown in Fig. 4 b, and CIE

coordinate is (0.2842, 0.2633). Different from the yellow light emitting from the aggregated solid compound sample, we speculated that the change of luminescence might be caused by some interaction between the solvent molecular DMA and the compound, and the combination of blue light and yellow light may lead to the final white light of compound 2. In order to more intuitively observe the fluorescence intensity of compound 2 in different solvents, the emission peak at 614 nm was separately plotted (See Fig. 4c).

3.8.2. Fluorescent sensing selectivity property

The luminescent responses of compound 2 were explored by treating 2@DMA suspensions (30 mg dispersed in 30 mL DMA) with 900 μ M different analytes such Fe³⁺, Al³⁺, Cu²⁺, Pb²⁺, Cd²⁺, Cr³⁺, Ba²⁺, Co³⁺, Ni²⁺, Mg²⁺, Zn²⁺, Ca²⁺, K⁺, Na⁺, respectively. First, 2 mL suspension was accurately removed to quartz cuvette with a pipette, and then 180 μ L of metal ions above were added to the system to test under the same conditions. Fluorescence intensities of suspensions containing above 14 kinds of metal ions were recorded and compared, as shown in Fig. 5a. Similarly, in order to more intuitive illustrate the fluorescent selectivity of the compound for different metal ions, we also compared the emission peaks at 614 nm, which could be attributed to the ⁵D₀-⁷F₂, as shown in Fig. 5b. It can be clearly seen that among the all detected metal ions, the fluorescence quenching ability of the compound 2 to Fe³⁺ is the strongest. Simultaneously, it should not

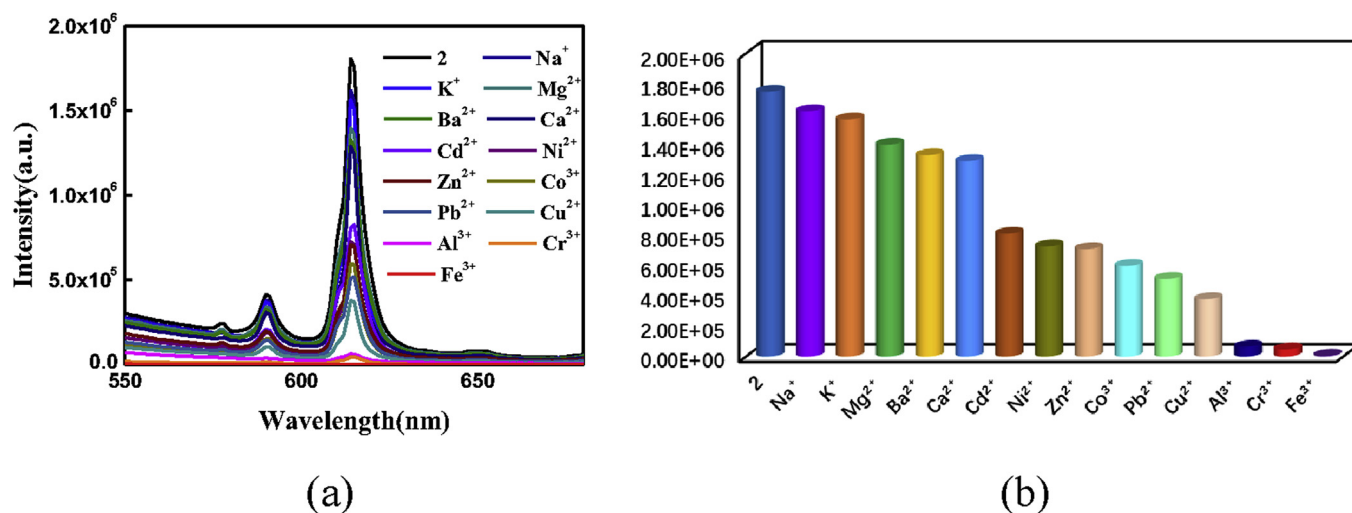


Fig. 5. Comparison of fluorescence intensity of compound 2 containing 14 different metal cations under the same conditions: (a) concentration-dependent curves; (b) fluorescence intensity histogram at 614 nm.

be neglected that the higher quenching effect of compound 2 on Al^{3+} and Cr^{3+} . In conclusion, it is shown that compound 2 has a good fluorescence quenching effect on Fe^{3+} , Al^{3+} , and Cr^{3+} , so it may be used as a fluorescence sensor that can detect three kinds of ions at the same time.

3.8.3. Sensitivity investigation

Due to Fe^{3+} , Al^{3+} and Cr^{3+} gave marked luminescence quenching effects, prompting us to explore the sensitivity of the compound 2 to Fe^{3+} , Al^{3+} and Cr^{3+} . The specific experimental method is as follows: the effect of the compound 2 on the fluorescence titration for Fe^{3+} , Al^{3+} and Cr^{3+} was further studied by sequentially adding 0–180 μL at a concentration of 10^{-2} mol/L to the suspension. It is excited to notice that remarkable quench effect were observed with the gradual addition of Fe^{3+} , Al^{3+} and Cr^{3+} and the quenching efficiency is about 99.70%, 96.20%, 97.30%, which were calculated by using the equation $(1 - I/I_0) \times 100\%$ (I_0 is the initial fluorescence intensity, I is the fluorescence intensity after addition ions) when the volume of three cations were added to 180 μL . The quenching rates are higher than reported quenching rates toward Fe^{3+} , Al^{3+} and Cr^{3+} , respectively, which indicate that the compound 2 has extremely excellent sensitivity to above three metal ions.

On this basis, in order to further explore the effect of compound 2 on the detection of lower concentrations of the test substance, we also diluted the concentration of three cations to 10^{-3} mol/L and performed the same titration experiment. The fluorescence intensity changes of compound 2 after adding three different volumes of metal cations respectively are shown in Fig. 6. The Stern-Volmer equation: $I_0/I = K_{sv}[Q] + 1$ (I_0 and I represent the fluorescence intensity before and after the addition of ions, respectively. K_{sv} is the quenching constant (M^{-1}), $[Q]$ represents the molar concentration of ions) can further explain the high sensitivity for Fe^{3+} , Al^{3+} and Cr^{3+} , by calculating the K_{sv} value of compound 2 to reach $1.77 \times 10^4 \text{ M}^{-1}$ ($R^2 = 0.9983$), $1.44 \times 10^4 \text{ M}^{-1}$ ($R^2 = 0.9982$), $3.621 \times 10^4 \text{ M}^{-1}$ ($R^2 = 0.95165$) according to the corresponding S-V plots, higher than previously reported compounds. The detection limit is another key data that indicate the sensitivity of the fluorescent probe. The detection limit are 1.93 μM , 2.38 μM , 0.945 μM corresponding to the above three metal ions, respectively, calculated by the formula: $3\sigma/K$ (σ is the standard deviation of the fluorescence intensity of the blank solution), lower than that reported in other compounds. The above data indicates that compound 2 is very promising as a potential fluorescence sensor to detect Fe^{3+} , Al^{3+} and Cr^{3+} in aqueous solution.

Aim at ascertain the compound 2 has the high sensing ability

towards Fe^{3+} , Al^{3+} and Cr^{3+} , interference experiments on three metal ions were performed separately, as shown in Fig. S5. Obviously, in the presence of other metal ions, the fluorescence quenching behavior is almost not affected, that is to say that the compound 2 is highly selective to Fe^{3+} , Al^{3+} and Cr^{3+} .

3.8.4. Sensing selectivity of compound 2 for different anions

Recognizing that the excellent fluorescence response of the compound 2 to metal ions drive us to further investigate whether it has the same remarkable detection effect on anions. So next, we will shift our focus to the fluorescence titration test for anions. 11 anionic solutions (Br^- , Ac^- , CO_3^{2-} , $\text{C}_2\text{O}_4^{2-}$, $\text{Cr}_2\text{O}_7^{2-}$, Cl^- , F^- , MnO_4^- , NO_3^- , PO_4^{3-} , SO_4^{2-}) with a concentration of 10^{-2} mol/L were prepared, respectively, the 180 μL solutions were accurately removed and dropped into the suspension containing 2 mg compound per 2 mL solution. The fluorescence intensity after each addition of different detection substance was recorded in time and the fluorescence quenching behavior was compared, the specific changes are shown in Fig. 7.

3.8.5. Sensitivity investigation of compound 2 for anions

It can be seen intuitively from Fig. 7 that compound 2 has better quenching behavior than other anions on four anions $\text{C}_2\text{O}_4^{2-}$, $\text{Cr}_2\text{O}_7^{2-}$, MnO_4^- , PO_4^{3-} , so then we did a concentration gradient test on four anions. Similarly, in the system DMA is used as a solvent, 2 mg compound 2 was dispersed in 2 mL DMA, and the suspension was formed by ultrasound for 30 min. Then 0–180 μL of four kinds of detection substances having a concentration of 10^{-2} mol/L was added sequentially into the suspension above. Fig. 8 shows the fluorescence intensity changes of the compound 2 with four anions added. In the same way, according to the Stern-Volmer equation: $I_0/I = K_{sv}[Q] + 1$, K_{sv} values of compounds with $\text{C}_2\text{O}_4^{2-}$, $\text{Cr}_2\text{O}_7^{2-}$, MnO_4^- , PO_4^{3-} were $2.07 \times 10^3 \text{ M}^{-1}$, $5.65 \times 10^3 \text{ M}^{-1}$, $3.18 \times 10^3 \text{ M}^{-1}$, $1.82 \times 10^3 \text{ M}^{-1}$, respectively. Therefore, according to the calculation of $3\sigma/K$, detection limits are 16.5 μM , 6.06 μM , 10.8 μM , 18.8 μM , respectively, lower than the detection limit of related ions previously reported.

Similarly, in order to explore whether other anions would interfere with the detected four ions $\text{C}_2\text{O}_4^{2-}$, $\text{Cr}_2\text{O}_7^{2-}$, MnO_4^- , PO_4^{3-} , we also conducted fluorescence interference experiments on the detected four anions. The experimental results are shown in Fig. S6. The results show that the other anions have almost no interference with the change of the fluorescence intensity of the four detected anions, indicating that the compound 2 has good selectivity for the four anions detected.

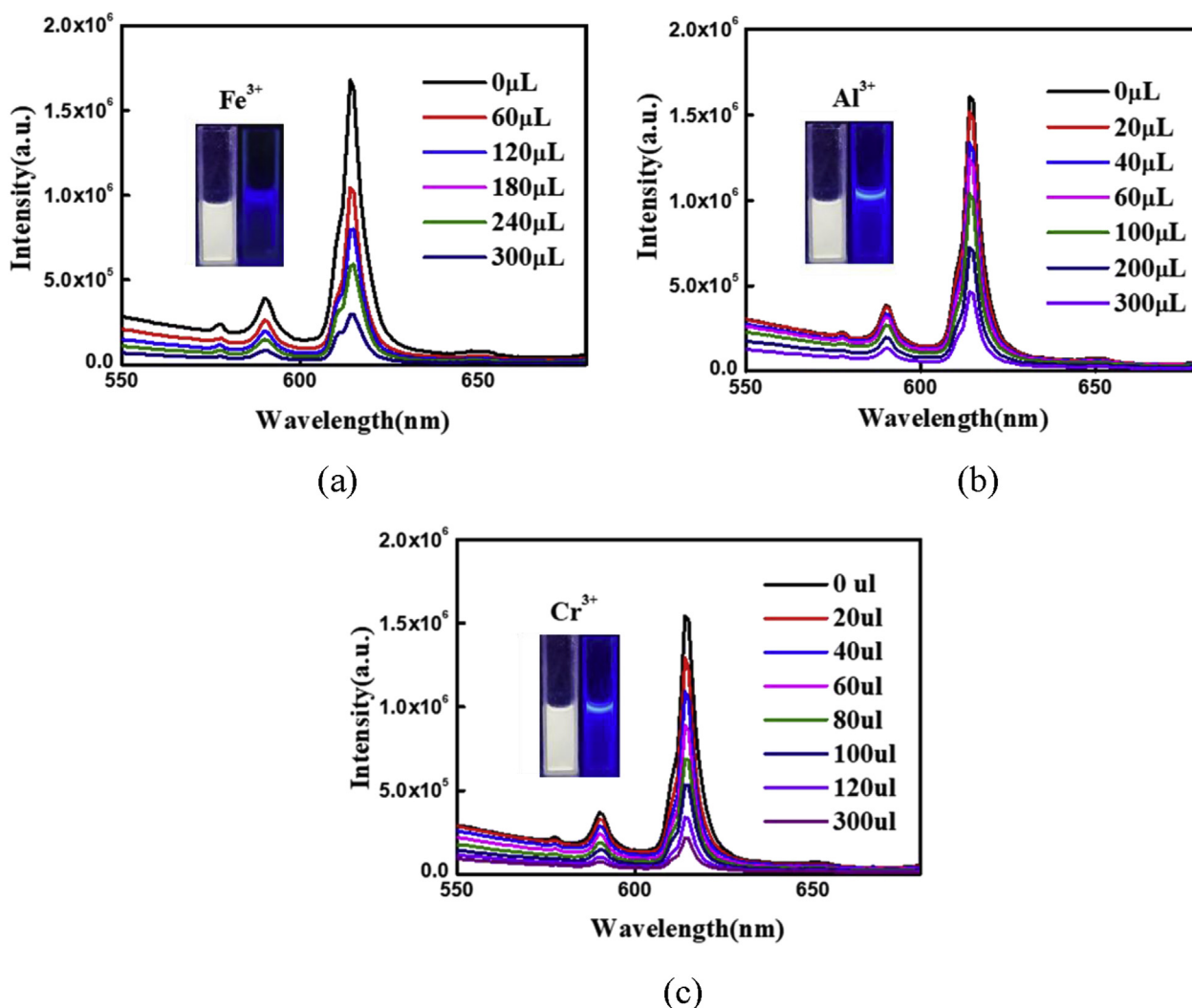


Fig. 6. Concentration-dependent luminescence intensities of compound 2 by the addition of different volumes of metal cation respectively, (a) Fe³⁺, (b) Al³⁺, (c) Cr³⁺ (Illustration: fluorescence quenching visible to the naked eye under ultraviolet light).

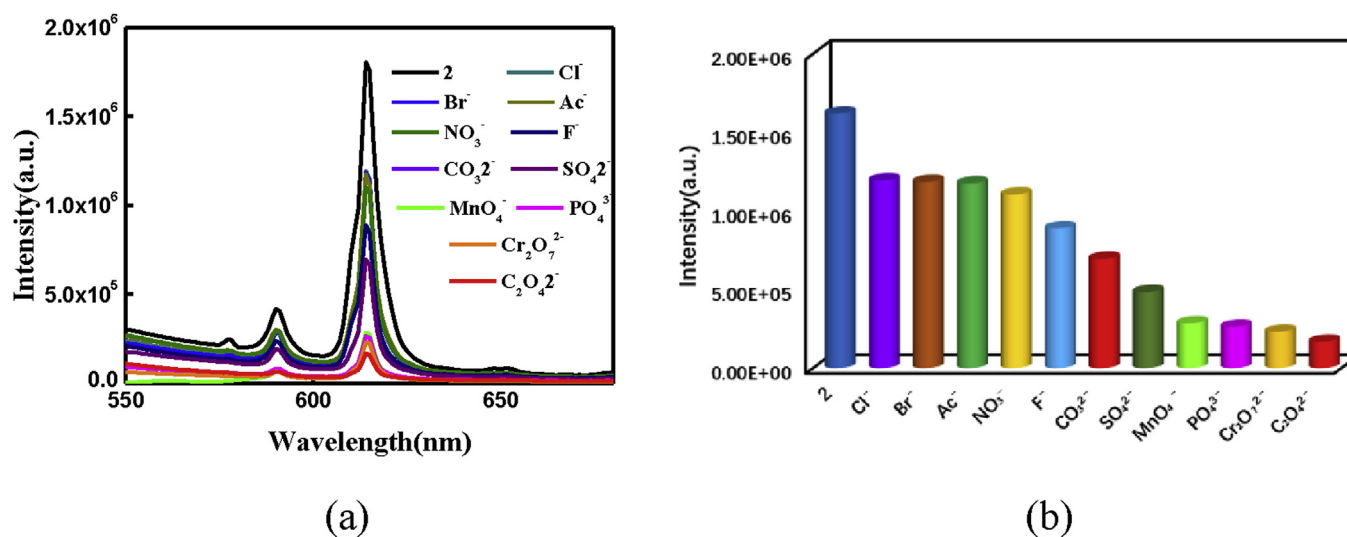


Fig. 7. (a) Comparison of fluorescence intensity of compound 2 containing 11 different anions under the same conditions: (a) concentration-dependent curves; (b) fluorescence intensity histogram at 614 nm.

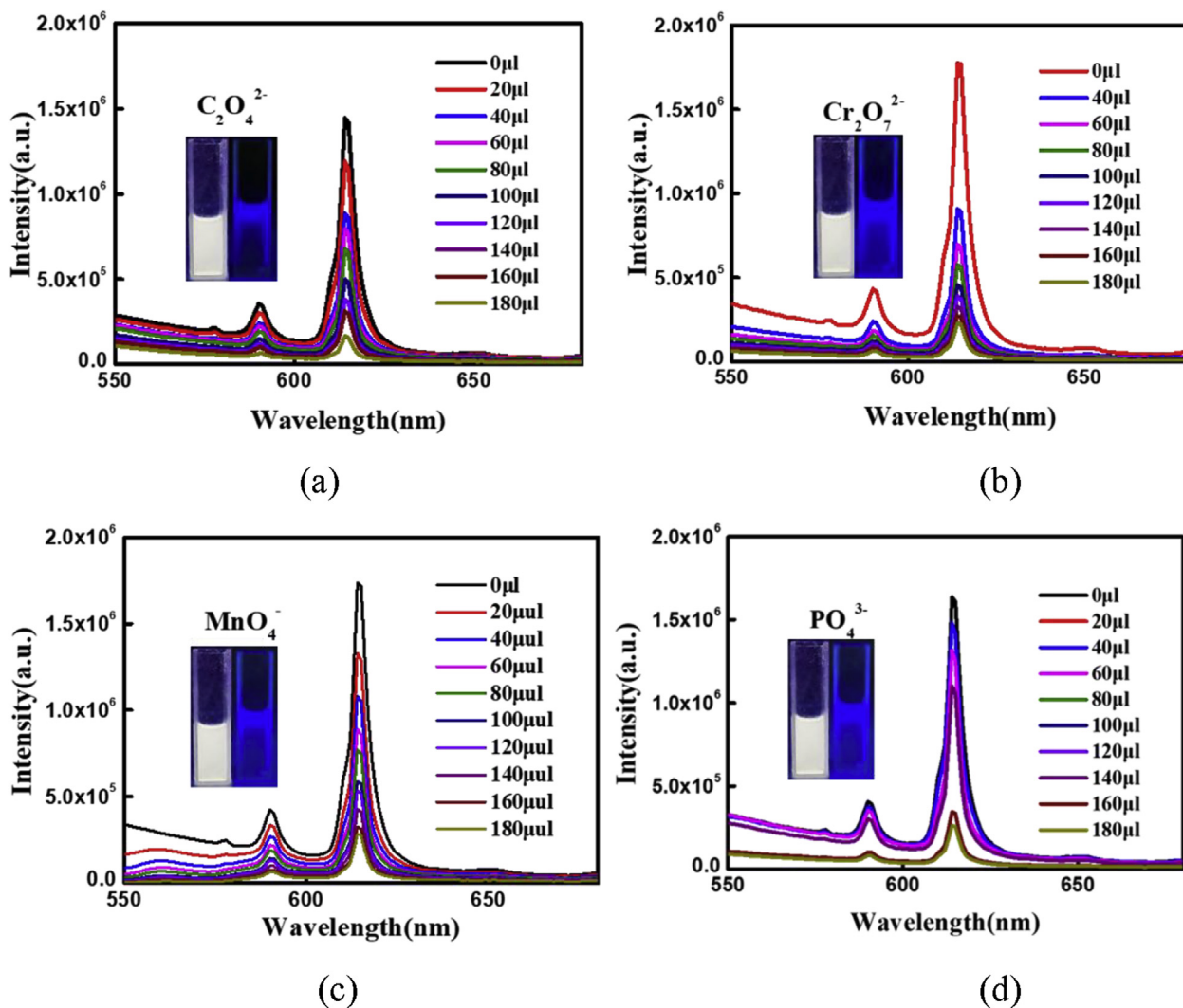


Fig. 8. The fluorescence intensity changes of compound 2 after adding four different volumes of anions respectively, (a) C₂O₄²⁻, (b) Cr₂O₇²⁻, (c) MnO₄⁻, (d) PO₄³⁻ (Illustration: fluorescence quenching visible to the naked eye under ultraviolet light).

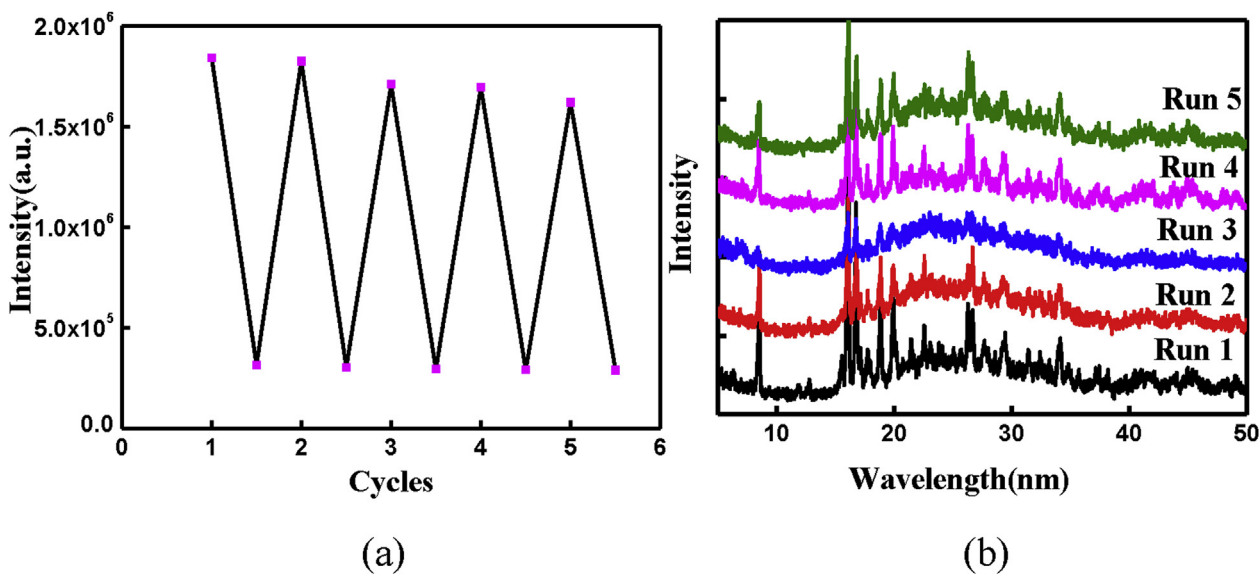


Fig. 9. (a) Cycle detection test of compound 2 for Fe³⁺; (b) PXRD spectra of five cycles of compound 2.

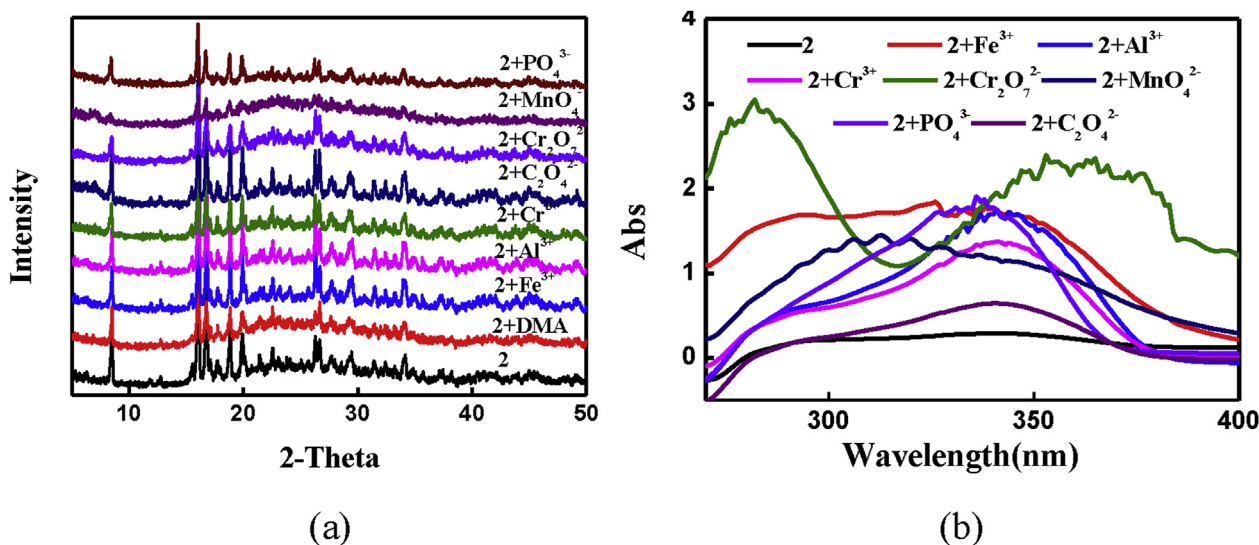


Fig. 10. (a) PXRD pattern of compound 2 after addition of various detection ions; (b) The UV-vis absorption spectra of the compound 2 before and after ions detection.

3.8.6. Study on the cyclability and stability of sensor based on compound 2

Superior cycle reusability and stability are indispensable parameters for high performance chemical sensors. In order to explore the recyclability of sensor (compound 2), the reproducibility study was performed through the fluorescence detection activity. We choose compounds with Fe^{3+} added recycled as an example, the specific operation is as follows: after adding 300 μL of Fe^{3+} to record the fluorescence intensity, compound 2 was recovered by centrifugation, washed with DMA and used for the next cycle, repeated test five times, compare the fluorescence intensity of each time. The change of fluorescence intensity before and after each addition of Fe^{3+} is shown in Fig. 9a. Since the fluorescence intensity of compound 2 dose not decreased obviously after five cycles, it is reasonable to believe that compound 2 can be used as an excellent cyclic material to detect Fe^{3+} . And, we also carried on the exploration to the stability of the compound 2, filter and dry the sample for each test, then to perform a PXRD test (Fig. 9b), the peak position in the spectrum can be well matched every time, show that compounds 2 has excellent stability. It is because of this kind of eminent stability, practicality and recycled, made compound 2 has a unique advantage act as fluorescent sensor testing materials.

3.8.7. Fluorescence respond mechanism

Studies have shown that there are generally several reasons lead to the fluorescence quenching of compounds: first, collapse of the skeleton of compound is a common way to quench the luminescence. For compound 2, the PXRD spectra before and after adding Fe^{3+} can be well matched (See Fig. 10a) reveal that the skeleton is still intact after the introduction of Fe^{3+} , indicating that the quenching caused by the collapse of the skeleton was excluded.

Secondly, the ligand H_2DLDA in compound 2 can effectively absorb the energy in the ultraviolet spectrum and transfer it to Eu^{3+} , so as to produce the characteristic luminescence spectrum of compound 2. Comparably, Fe^{3+} shows nonnegligible photon-absorption at 270–400 nm (as shown in Fig. 10b), suggesting that the introduction of Fe^{3+} have obvious effect on the energy absorption of the ligand, which means excited photons are absorbed by Fe^{3+} , which prohibits efficient energy transfer from the ligand to the Eu^{3+} , and ultimately results in luminescence.

Third, the collision interaction between compound 2 and free Fe^{3+} ions may consume the energy and reduce the luminescent intensity. From the framework of the compound, we know that the presence of multiple conjugated π electrons in the structure due to the direct

connection of multiple benzene rings. In the process of binding with Fe^{3+} , the electron donating ability of the compound is enhanced by the excited state delocalized π^* electrons, which facilitates exciton migration and increases the electrostatic effect of the compound and Fe^{3+} . Since there are multiple sites in the conjugated compound, when Fe^{3+} acts as a receptor and binds to one of the sites, it will transfer along the conjugated chain, causing multiple sites to respond at the same time, and then effective quenching occurs.

In addition, the SV plots of the Fe^{3+} shows a linear relationship in the lower concentration region, while a nonlinear relationship was obtained in the higher concentration region (See Fig. 11. See Fig. S7 and Fig. S8 for the SV plots of other detected ions). This nonlinear relationship at higher concentrations indicates simultaneous dynamic quenching and static quenching or resonance energy transfer behavior. To better understand the fluorescence quenching mechanism, fluorescent lifetime values for the compound 2 were performed in the DMA suspension before and after the addition of Fe^{3+} to determine the type of reaction quenching (See Fig. 12). Theoretically, dynamic quenching is caused by the decrease of fluorescence intensity due to the collision between the quencher and the fluorophore, which results in a decrease in the lifetime, while static quenching is caused by the combination of the quenching agent and fluorophore to produce substances that do not produce fluorescence. The existence of quenching agent does not

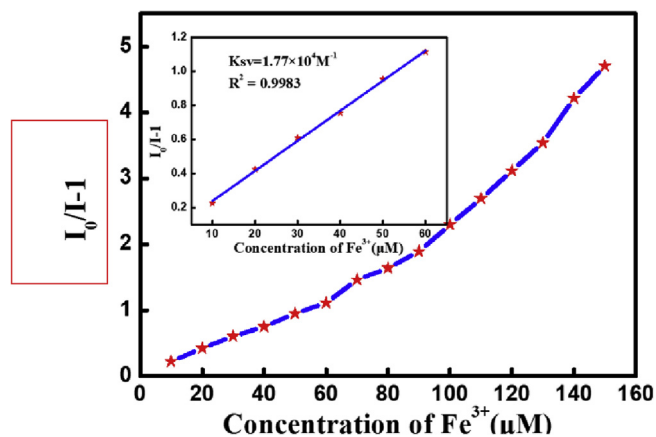


Fig. 11. The fitting curves of the nonlinear S-V plots of 2 for various concentrations of Fe^{3+} by the exponential quenching equation. Inset: the fitting curves of the linear S-V plots for Fe^{3+} at low concentrations.

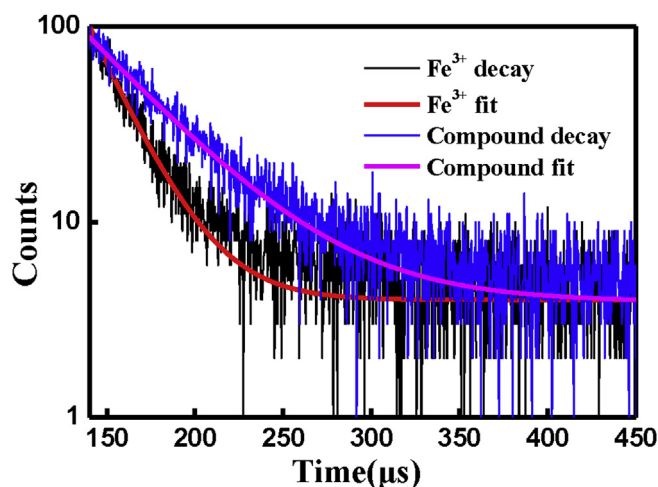


Fig. 12. The change of lifetime curves before and after Fe^{3+} .

change the lifetime of fluorescence molecular excitation state. After Fe^{3+} was added, the corresponding lifetime value decreased from 335 μs to 239 μs , indicating that dynamic quenching was dominant in the whole quenching process, which is consistent with the conclusions illustrated in SV plots. In addition, the quenching mechanism of compound can be further determined by absorption spectra. Dynamic quenching mainly affects the excited state of the fluorescence molecule, so it does not affect the absorption spectrum of the fluorescence substance, while in static quenching, the characterization of ground state of the compounds often changes the absorption spectrum of the material. However, when Fe^{3+} was added, the absorption peak of compound 2 did not shift, which further proved that the quenching type of compound 2 was dominated by dynamic quenching.

In addition, in the case of anions and cations, the UV-Vis spectrum displays apparent absorption ranging from 300 to 370 nm (Fig. 10b), which also has a large overlap with the excitation spectrum of 2. Furthermore, many C atoms and uncoordinated O atoms exist in 2, which could act as hydrogen bonds donors and acceptors to enhance the interactions between detector and 2. Meanwhile, there are many benzene rings in 2, which may form the π - π stacking interactions with detectors. Consequently, the electrostatic interactions and energy-transfer could occur between 2 and detector supported by the exponential S-V curve of detector, which may be another probable reason for the luminescent quenching.

Thus, a possible quenching mechanism is proposed as follows: the introduction of Fe^{3+} may consume the energy through the collision interaction and further decrease the energy transfer from H_2DLDA to Eu^{3+} centers, resulting in the luminescence quenching of compound 2. The luminescence quenching mechanism of Fe^{3+} was discussed in detail, which could be used as a model for other ions.

4. Conclusions

In a word, by rare earth Eu^{3+} ions and fluorene derivatives, the successful preparation of a kind of new fluorescent probe materials, $[\text{Eu}(\text{DLDA})(\text{DMF})(\text{H}_2\text{O})(\text{COO})]_n$, which can simultaneously detect a variety of metal ions and the anion in the solution. By fluorescence titration experiment proved that the compound has extremely high sensitivity and very low detection limit, and outstanding chemical stability, and distinct fluorescence quenching is visible to the naked eye under UV light. Moreover, the mechanism of its quenching is explained to some extent. It is expected to enrich the application of fluorene and its derivatives in the field of photoluminescence, has a wide application prospect. In addition, through the same method, the other four rare earth compounds were also successfully synthesized. A series of characterizations proved that they are isomorphous compounds with Eu

DLDA compound and have 3D supramolecular network structural characterization.

Accession codes

CCDC for the compound 1:1914134 contain the supplementary crystallographic data for this paper. These data can be obtained free of charge via www.ccdc.cam.ac.uk/data_request/cif, or by emailing data_request@ccdc.cam.ac.uk, or by contacting The Cambridge Crystallographic Data Centre, 12 Union Road, Cambridge CB2 1EZ, UK; fax: +44 1223 226033.

Acknowledgements

This work was supported by the grants of the National Natural Science Foundation of China (No. 21571091), Commonweal Research Foundation of Liaoning province in China (No. 20170055) for financial assistance for financial assistance.

Appendix A. Supplementary data

Supplementary data to this article can be found online at <https://doi.org/10.1016/j.dyepig.2019.107862>.

References

- [1] Papaefstathiou GS, MacGillivray LR. Inverted metal-organic frameworks: solid-state hosts with modular functionality. *Coord Chem Rev* 2003;246:169–84.
- [2] Zaworotko M. Nanoporous structures by design. *Angew Chem* 2000;39:3052.
- [3] Yaghi OM, O'Keeffe M, Kanatzidis M. Design of solids from molecular building blocks: golden opportunities for solid state chemistry. *J Solid State Chem* 2000;152:1–2.
- [4] Noveron JC, Lah MS, Del Sesto RE, Arif AM, Miller JS, Stang PJ. Engineering the structure and magnetic properties of crystalline solids via the metal-directed self-assembly of a versatile molecular building unit. *J Am Chem Soc* 2002;124:6613–25.
- [5] Yang H, Li JR. Metal-organic frameworks (MOFs) for CO_2 capture porous materials for carbon dioxide capture. Berlin, Heidelberg: Springer; 2014. p. 79–113.
- [6] Eddaoudi M, Moler DB, Li HL, Chen BL, Reineke TM, O'Keeffe M, Yaghi OM. Modular chemistry: secondary building units as a basis for the design of highly porous and robust metal-organic carboxylate frameworks. *Accounts Chem Res* 2001;34:319–30.
- [7] Evans OR, Lin W. Crystal engineering of NLO materials based on metal-organic coordination networks. *Accounts Chem Res* 2002;35:511–22.
- [8] Hao JN, Yan B. Amino-decorated lanthanide (III) organic extended frameworks for multi-color luminescence and fluorescence sensing. *J Mater Chem C* 2014;2:6758–64.
- [9] Li JR, Kuppler RJ, Zhou HC. Selective gas adsorption and separation in metal-organic frameworks. *Chem Soc Rev* 2009;38:1477–504.
- [10] Kalidindi SB, Oh H, Hirscher M, Esken D, Wiltor C, Turner S, Tendeloo GV. Metal@COFs: covalent organic frameworks as templates for Pd nanoparticles and hydrogen storage properties of Pd@COF-102 hybrid material. *Chem Eur J* 2012;18:10848–56.
- [11] Guo YX, Feng X, Han TY, Wang S, Lin ZG, Dong YP, Wang B. Tuning the luminescence of metal-organic frameworks for detection of energetic heterocyclic compounds. *J Am Chem Soc* 2014;136:15485–8.
- [12] Jiang HL, Feng DW, Liu TF, Lin JR, Zhou HC. Pore surface engineering with controlled loadings of functional groups via click chemistry in highly stable metal-organic frameworks. *J Am Chem Soc* 2012;134:14690–3.
- [13] Sumida K, Rogov DL, Mason JA, McDonald TM, Bloch ED, Herm ZR, Bae TH, Long JR. Carbon dioxide capture in metal-organic frameworks. *Chem Rev* 2011;112:724–81.
- [14] Amarante SF, Freire MA, Mendes DTSL, Freitas LS, Ramos ALD. Evaluation of basic sites of ZIFs metal organic frameworks in the Knoevenagel condensation reaction. *Appl Catal Gen* 2017;548:47–51.
- [15] Tan K, Nijem N, Canepa P, Gong QH, Li J, Thonhauser T, Chabal YJ. Stability and hydrolyzation of metal organic frameworks with paddle-wheel SBUs upon hydration. *Chem Mater* 2012;24:3153–67.
- [16] Ma S, Zhou HC. Gas storage in porous metal-organic frameworks for clean energy applications. *Chem Commun* 2010;46:44–53.
- [17] Wu HH, Gong QH, Olson DH, Li J. Commensurate adsorption of hydrocarbons and alcohols in microporous metal organic frameworks. *Chem Rev* 2012;112:836–68.
- [18] Zhou HC, Long JR, Yaghi OM. Introduction to metal-organic frameworks. *Chem Rev* 2012;112:673–4.
- [19] Plessius R, Kromhout R, Ramos ALD, Ferbinteanu M, Mittelmeijer-Hazeleger MC, Krishna R, Rothenberg G, Tanase S. Highly selective water adsorption in a lanthanum metal-organic framework. *Chem Eur J* 2014;20:7922–5.
- [20] Mukherjee S, Ganguly S, Chakraborty A, Mandal A, Das D. Green synthesis of self assembled nanospherical dysprosium MOFs: selective and efficient detection of

- picric acid in aqueous and gas phase. *Sustainable Chem Eng* 2018;7:819–30.
- [21] Müller-Buschbaum K, Beuerle F, Feldmann C. MOF based luminescence tuning and chemical/physical sensing. *Microporous Mesoporous Mater* 2015;216:171–99.
- [22] Rieutord A, Prognon P, Brion F, Mahuzier G. Liquid chromatographic determination using lanthanides as time-resolved luminescence probes for drugs and xenobiotics: advantages and limitations. *Analyst* 1997;122:59R–66R.
- [23] Duan TW, Yan B. Hybrids based on lanthanide ions activated yttrium metal–organic frameworks: functional assembly, polymer film preparation and luminescence tuning. *J Mater Chem C* 2014;2:5098–104.
- [24] Song XZ, Song SY, Zhao SN, Hao ZM, Zhu M, Meng X, Wu LL, Zhang HJ. Single-Crystal-to-Single-Crystal transformation of a europium (III) metal–organic framework producing a multi-responsive luminescent sensor. *Adv Funct Mater* 2014;24:4034–41.
- [25] Huang LS, Lin KC. Detection of iron species using inductively coupled plasma mass spectrometry under cold plasma temperature conditions. *Spectrochim Acta B At Spectrosc* 2001;56:123–8.
- [26] Wu P, Li Y, Yan XP. CdTe quantum dots (QDs) based kinetic discrimination of Fe^{2+} and Fe^{3+} , and CdTe QDs-fenton hybrid system for sensitive photoluminescent detection of Fe^{2+} . *Anal Chem* 2009;81:6252–7.
- [27] Rieutord A, Prognon P, Brion F, Mahuzier G. Liquid chromatographic determination using lanthanides as time-resolved luminescence probes for drugs and xenobiotics: advantages and limitations. *Analyst* 1997;122:59R–66R.
- [28] Dang S, Ma E, Sun ZM, Zhang HJ. A layer-structured Eu-MOF as a highly selective fluorescent probe for Fe^{3+} detection through a cation-exchange approach. *J Mater Chem* 2012;22:16920.
- [29] Liu JQ, Li GP, Liu WC, Li QL, Li BH, Gable RW, Hou L, Batten SR. Two unusual nanocage-based In-MOFs with triazole sites: highly fluorescent sensing for Fe^{3+} and $\text{Cr}_2\text{O}_7^{2-}$, and selective CO_2 capture. *ChemPlusChem* 2016;81:1299–304.
- [30] Hu Z, Deibert BJ, Li J. Luminescent metal-organic frameworks for chemical sensing and explosive detection. *Chem Soc Rev* 2014;43:5815–40.
- [31] Li CR, Hai J, Li SL, Wang BD, Yang ZY. Luminescent magnetic nanoparticles encapsulated in MOFs for highly selective and sensitive detection of $\text{ClO}^-/\text{SCN}^-$ and anti-counterfeiting. *Nanoscale* 2018;10:8667–76.
- [32] Ni R, Tong RB, Guo CC, Shen GL, Yu RQ. An anthracene/porphyrin dimer fluorescence energy transfer sensing system for picric acid. *Talanta* 2004;63:251–7.
- [33] Imai K, Kihara Y, Kimoto A, Abe J, Tamai Y, Nemoto N. Synthesis and characterization of poly(tetramethylsilylarylenesiloxane) derivatives bearing diphenylfluorene or diphenyldibenzosilole moieties. *Polym J* 2010;43:58–65.
- [34] Neher D. Polyfluorene homopolymers: conjugated liquid-crystalline polymers for bright blue emission and polarized electroluminescence. *Macromol Rapid Commun* 2015;22:1365–85.
- [35] Wong KT, Chien YY, Chen RT, Wang CF, Lin YT, Chiang HH, Hsieh PY, Wu CC, Chou CH, Su YO, Lee GH, Peng SM. Ter (9, 9-diarylfuorene)s: highly efficient blue emitter with promising electrochemical and thermal stability. *J Am Chem Soc* 2002;124:11576–7.
- [36] Cho NS, Park JH, Lee SK, Lee JH, Shim HK, Park MJ, Hwang DH, Jung BJ. Saturated and efficient red light-emitting fluorene-based alternating polymers containing phenothiazine derivatives. *Macromolecules* 2006;39:177–83.
- [37] Scherf U, List EJW. Semiconducting polyfluorenes-towards reliable structure-property relationships. *Adv Mater* 2002;14:477–87.
- [38] Moreau F, Audebrand N, Poriol C, Baslé VM, Ouvry J. A 9,9'-spirobifluorene based Metal–Organic Framework: synthesis, structure analysis and gas sorption properties. *J Mater Chem* 2011;21:18715–22.
- [39] Tao SL, Peng ZK, Zhang XH, Wang PF, Lee C-S. Highly efficient non-doped blue organic light-emitting diodes based on fluorene derivatives with high thermal stability. *Adv Funct Mater* 2005;15:1716–21.
- [40] Donat-Bouillud A, Lévesque I, Tao Y, D'lorio M, Beaupré S, Blondin P, Ranger M, Bouchard J, Leclerc M. Light-emitting diodes from fluorene-based π -conjugated polymers. *Chem Mater* 2000;12:1931–6.
- [41] Vallejos S, Kaoutit HE, Estévez P, García FC, Peña JL, Serna F, García JM. Working with water insoluble organic molecules in aqueous media: fluorene derivative-containing polymers as sensory materials for the colorimetric sensing of cyanide in water. *Polym Chem* 2011;2:1129–38.
- [42] Lim E, Jung BJ, Lee J, Shim HK, Lee JI, Yang YS, Do LM. Thin-film morphologies and solution-processable field-effect transistor behavior of a fluorene-thieno [3,2-b] thiophene-based conjugated copolymer. *Macromolecules* 2005;38:4531–5.
- [43] Yi L, Shi LL, Feng JK, Yang L, Ren AM. Luminescent properties of mercury-taining diethynylfluorene derivatives. *Chem Res Chin Univ* 2007;23:92–5.
- [44] Belfield KD, Morales AR, Kang BS, Hales JM, Hagan DJ, Stryland EWW, Chapela VM, Percino J. Synthesis, characterization, and optical properties of new two-photon-absorbing fluorene derivatives. *Chem Mater* 2004;16:4634–41.
- [45] Miteva T, Meisel A, Knoll W, Nothofer HG, Scherf U, Müller DC, Meerholz K, Yasuda A, Neher D. Improving the performance of polyfluorene-based organic light-emitting diodes via end-capping. *Adv Mater* 2001;13:565–70.
- [46] Li L, Wang Z, Chen Q, Zhou XH, Yang T, Zhao Q, Huang W. Coordination polymers assembled from semirigid fluorene-based ligand: a couple of enantiomers. *J Solid State Chem* 2015;231:47–52.
- [47] Aragay G, Pons J, Merkoçi A. Recent trends in macro-, micro-, and nanomaterial-based tools and strategies for heavy-metal detection. *Chem Rev* 2011;111:3433–58.
- [48] Kumari S, Panda C, Mazumdar S, Gupta SS. A molecular Fe-compound as a catalyst probe for in-gel visual detection of proteins via signal amplification. *Chem Commun* 2015;51:15257–60.
- [49] Hou YL, Xu H, Cheng RR, Zhao B. Controlled lanthanide–organic framework nanospheres as reversible and sensitive luminescent sensors for practical applications. *Chem Commun* 2015;51:6769–72.
- [50] Xu H, Zhai B, Cao CS, Zhao B. A bifunctional europium–organic framework with chemical fixation of CO_2 and luminescent detection of Al^{3+} . *Inorg Chem* 2016;55:9671–6.
- [51] Xu H, Cao CS, Zhao B. A water-stable lanthanide-organic framework as a recyclable luminescent probe for detecting pollutant phosphorus anions. *Chem Commun* 2011;51:10280–3.
- [52] Xu H, Xiao YQ, Rao XT, Dou ZS, Li WF, Gui YJ, Wang ZY, Qian GD. A metal-organic framework for selectively sensing of PO_4^{3-} anion in aqueous solution. *J Alloy Comp* 2011;509:2552–4.
- [53] Shi PF, Zhao B, Xiong G, Hou YL, Cheng P. Fast capture and separation of, and luminescent probe for, pollutant chromate using a multi-functional cationic heterometal-organic framework. *Chem Commun* 2012;48:8231–3.
- [54] Tian HR, Gao CY, Yang Y, Ai J, Liu C, Xu ZG, Sun ZM. A microporous Cd-MOF based on a hexavalent silicon-centred connector and luminescence sensing of small molecules. *New J Chem* 2017;41:1137–41.
- [55] Cao KL, Xia Y, Wang GX, Feng YL. A robust luminescent Ba (II) metal–organic framework based on pyridine carboxylate ligand for sensing of small molecules. *Inorg Chem Commun* 2015;53:42–5.
- [56] Li HQ, Ding ZY, Pan Y, Liu CH, Zhu YY. Fluorescence tuning of Zn (II)-based metallo-supramolecular coordination polymers and their application for picric acid detection. *Inorg Chem Front* 2016;3:1363–75.
- [57] Maiti K, Mahapatra AK, Gangopadhyay A, Maji R, Mondal S, Ali SS, Das S, Sarkar R, Datta P, Mandal D. Simple bithiocarbonohydrazone as a sensitive, selective, colorimetric, and ratiometric fluorescent chemosensor for picric acids. *ACS Omega* 2017;2:1583–93.
- [58] Allendorf MD, Bauer CA, Bhakta RK, Houk RJT. Luminescent metal-organic frameworks. *Chem Soc Rev* 2009;38:1330–52.
- [59] Wang XN, Li JL, Jiang CG, Hu P, Li B, Zhang T, Zhou HC. An efficient strategy for improving the luminescent sensing performance of a terbium (III) metal–organic framework towards multiple substances. *Chem Commun* 2018;54:13271–4.
- [60] Jing T, Chen L, Jiang FL, Yang Y, Zhou K, Yu MX, Cao Z, Li SC, Hong MC. Fabrication of a robust lanthanide metal–organic framework as a multifunctional material for Fe (III) detection, CO_2 capture, and utilization. *Cryst Growth Des* 2018;18:2956–63.
- [61] Li GP, Liu G, Li YZ, Hou L, Wang YY, Zhu ZH. Uncommon pyrazolyl-carboxyl bi-functional ligand-based microporous lanthanide systems: sorption and luminescent sensing properties. *Inorg Chem* 2016;55:3952–9.
- [62] Wang Y, Xing SH, Bai FY, Xing YH, Sun LY. Stable lanthanide–organic framework materials constructed by a triazolyl carboxylate ligand: multifunction detection and white luminescence tuning. *Inorg Chem* 2018;57:12850–9.
- [63] Huang YQ, Chen HY, Wang Y, Ren YH, Li ZG, Li LC, Wang Y. A channel-structured Eu-based metal–organic framework with a zwitterionic ligand for selectively sensing Fe^{3+} ions. *RSC Adv* 2018;8:21444–50.
- [64] Chen Z, Sun YW, Zhang LL, Sun D, Liu FL, Meng QG, Wang RM, Sun DF. A tubular europium–organic framework exhibiting selective sensing of Fe^{3+} and Al^{3+} over mixed metal ions. *Chem Commun* 2013;49:11557–9.
- [65] Zheng M, Tan HQ, Xie ZG, Zhang LG, Jing XB, Sun ZC. Fast response and high sensitivity europium metal organic framework fluorescent probe with chelating terpyridine sites for Fe^{3+} . *ACS Appl Mater Interfaces* 2013;5:1078–83.
- [66] Shaya J, Deschamps MA, Michel BY, Burger A. Air-stable Pd catalytic systems for sequential one-pot synthesis of challenging unsymmetrical aminoaromatics. *J Org Chem* 2016;81:7566–73.
- [67] Ni YC. Synthesis of novel functional fluorene compounds and triazoles and their fluorescence sensing properties[D]. Liaoning: Liaoning normal university; 2017.
- [68] Sheldrick GM. A short history of SHELX. *Acta Crystallogr A: Found Crystallogr* 2008;64:112–22.
- [69] Sheldrick GM. SADABS, program for empirical absorption correction for area detector data. Gottingen, Germany: University of Gottingen; 1996.
- [70] Sheldrick GM. SHELXS 97, program for crystal structure refinement. Gottingen, Germany: University of Gottingen; 1997.
- [71] Burrows AD, Cassar K, Friend RMW, Mahon MF, Rigby S, Warren JE. Solvent hydrolysis and templating effects in the synthesis of metal-organic frameworks. *CrysolEngComm* 2005;7:548–50.
- [72] Chen L, Zhang H, Pan M, Wei ZW, Wang HP, Fan YN, Su CY. An efficient visible and near-infrared (NIR) emitting Sm (III) metal–organic framework (Sm-MOF) sensitized by excited-state intramolecular proton transfer (ESIPT) ligand. *Chem Asian J* 2016;11:1765–9.
- [73] Ni JC, Yan J, Zhang LJ, Shang D, Du N, Li S, Zhao JX, Wang Y, Xing YH. Bifunctional fluorescent quenching detection of 2, 4, 6-trinitrophenol (TNP) and acetate ions via a 4'-(9, 9-dimethyl-9H-fluorene-2, 7-diyl) dibenzoic acid. *Tetrahedron Lett* 2016;57:4978–82.